Hydrodynamic suppression of phase separation in active suspensions

Ricard Matas-Navarro,[1] Ramin Golestanian,[2] Tanniemola B. Liverpool,[3] and Suzanne M. Fielding[1,*]
[1]*Department of Physics, University of Durham, Science Laboratories, South Road, Durham, DH1 3LE, UK*
[2]*Rudolf Peierls Centre for Theoretical Physics, University of Oxford, Oxford, OX1 3NP, UK*
[3]*School of Mathematics, University of Bristol, Clifton, Bristol, BS8 1TW, UK*
(Received 19 October 2012; revised manuscript received 21 July 2014; published 18 September 2014)

We simulate with hydrodynamics a suspension of active disks squirming through a Newtonian fluid. We explore numerically the full range of squirmer area fractions from dilute to close packed and show that "motility induced phase separation," which was recently proposed to arise generically in active matter, and which has been seen in simulations of active Brownian disks, is strongly suppressed by hydrodynamic interactions. We give an argument for why this should be the case and support it with counterpart simulations of active Brownian disks in a parameter regime that provides a closer counterpart to hydrodynamic suspensions than in previous studies.

DOI: 10.1103/PhysRevE.90.032304 PACS number(s): 64.75.Jk, 87.18.Hf, 05.40.−a

I. INTRODUCTION

"Active matter" [1] comprises internal subunits that collectively drive the system far from Boltzmann equilibrium by each individually consuming energy. Biological examples include actively cross-linked polymeric filaments in the cell cytoskeleton [2], cells grouped in living tissues [3], suspensions of motile microorganisms [4,5], and shoals of fish and flocks of birds [6]. Nonbiological examples include vibrated granular monolayers [7–9] and self-propelled synthetic colloidal particles [10,11].

Distinct from the more familiar scenario of a passive complex fluid driven by, say, a global shear flow imposed at the system's boundaries, in active matter the driving out of equilibrium arises intrinsically in the active subunits throughout the system's own bulk. Consequently active materials can spontaneously develop mesoscopic or macroscopic mechanical stresses and deformations even without driving or loading from outside. Other exotic and generically emergent phenomena include swarming, pattern formation, giant number fluctuations, nonequilibrium ordering, and phase separation (for a recent review see Ref. [1]). These offer fascinating challenges to fluid dynamicist, rheologist, and statistical physicist alike.

Many active particles are elongated and so have an intrinsic (steric) tendency to align with each other [12–16]. Activity-mediated coupling between these orientational modes and fluctuations in the local number density then provide a generic mechanism for giant number fluctuations and phase separation [7,9,17]. The standard deviation ΔN in a subregion of material of mean number of particles N then scales as N^a with $a > 1/2$, whereas for passive systems away from any transition $a = 1/2$.

Besides any such tendency for alignment, another generic mechanism for phase separation was recently put forward in the context of "run and tumble" particles, such as some species of motile bacteria [18,19]. These swim in nearly straight-line runs at almost constant speed, between intermittent tumbles in which they suddenly randomize swim direction. The basic idea is that particles (a) accumulate where they move more slowly and (b) move more slowly where crowded. Positive feedback between (a) and (b) then gives rise to "motility-induced phase separation" (MIPS). This idea was recently extended analytically to active Brownian particles [20], consistent with simulations showing phase separation in active Brownian disks [21] and spheres [22] that indeed lack any tendency for steric alignment, or for phase separation in the passive equilibrium case.

To date these simulations lack hydrodynamic interactions, in which moving particles set up flow fields that influence their neighbors. But such interactions arise widely in active matter [1], and this is fundamentally important because steady state properties in nonequilibrium systems depend strongly on dynamics, in contrast to equilibrium states, which depend only on the underlying free energy. This includes the existence (or otherwise) of activity-induced phase separation.

The contribution of this work is to show that hydrodynamic interactions in fact strongly suppress MIPS. Accordingly, MIPS might not arise as generically in active matter as hitherto suggested. We show this by simulating with hydrodynamics a suspension of active disks [23–25] that squirm through a Newtonian fluid. A closely related model was studied previously in [26–28]. We explore the full range of squirmer area fractions from dilute to close packed and demonstrate that hydrodynamics causes a key assumption of the (a)–(b) feedback mechanism outlined above to fail. It does so by effectively rendering a crucial parameter (defined below) $\zeta \approx 1$ rather than $\zeta \gg 1$. To support this, we further demonstrate suppression of MIPS in active Brownian disks in the regime $\zeta \approx 1$ more closely analogous to the squirmers, with MIPS recovered for $\zeta \gg 1$, as explored previously for active Brownian particles [21].

Being disks, the active particles studied here lack any steric tendency to align with each other. This choice was made deliberately in order to exclude *a priori* the first, non-MIPS mechanism for active phase separation discussed above. For simulations of active rods with hydrodynamics, see Ref. [29].

The paper is structured as follows. In Sec. II we outline the models to be studied in the rest of paper. In Sec. III we detail our simulation methods. Units and parameter values are discussed in Sec. IV, then the statistical quantities that we measure from the simulations are defined in Sec. V. In Sec. VI we present

*suzanne.fielding@durham.ac.uk

our results, and we provide a discussion of them in Sec. VII. Finally in Sec. VIII we give conclusions and perspectives for future study.

II. MODELS

In this section we outline the models to be studied throughout the manuscript. We start in Secs. II A and II B by discussing hydrodynamic squirmers, before summarizing in Sec. II C the active Brownian particles that we shall simulate for comparison with the hydrodynamic case.

A. Squirmers

The model of hydrodynamic swimmers that we shall adopt is based on a minimal description of microbial propulsion originally put forward by Lighthill [23], then further by Blake [24,25], and studied extensively by Pedley *et al.* [26,28]. The swimming particles are assumed to be neutrally buoyant and so force free. Their size and swimming speed are assumed sufficiently small that the Reynolds number is negligible, and the flow associated with their swimming is Stokesian. Their size is, however, assumed large enough that Brownian motion is negligible (infinite Péclet number).

Swimming through the suspending fluid is achieved by means of an imposed tangential squirming velocity around the particle surface, but without changing the particle shape. This is intended to mimic, for example, locomotion by the beating of many cilia on the surface of a ciliated microbe. For simplicity the tangential velocity is assumed time independent, representing an average over many beating cycles. Spherical (three-dimensional, 3D) [24] and cylindrical (two-dimensional, 2D) [25] incarnations of this model have been considered, with axisymmetric tangential velocity assumed for the spherical case.

The model adopted here is based on the 2D model as put forward by Blake (i.e., infinitely long cylinders). We shall then further adapt it to the case of a film of disks (i.e., highly flattened cylinders) to give a model that has 3D hydrodynamics.

B. Squirming disks

We consider an ensemble of P inertialess disklike particles, each of radius R, actively propelling themselves in the x-y plane of a horizontal film of an inertialess, incompressible Newtonian fluid of viscosity η. The film has dimensions L_x, L_y, with periodic boundary conditions in the x and y directions. The disks and the film each have height h, with the top and the bottom of the film at $z = \pm h/2$. Semi-infinite volumes of a Newtonian fluid of a lower viscosity $\eta_0 < \eta$ fill the space above and below the film (see Fig. 1). This geometry was first considered by Saffman and Delbruck in the context of protein diffusion in fluid membranes [30–33]. One can define the Saffman length as $\ell = \eta h/\eta_0$, which quantifies the relative significance of the viscous dissipation in the 2D film as compared with the 3D dissipation in the bulk. As a simple rule of thumb, one can imagine an effective description of the hydrodynamic interactions between the disks, by regarding them as objects of typical size set by the Saffman length that would interact through 3D bulk viscous hydrodynamics (see Figs. 1 and 2).

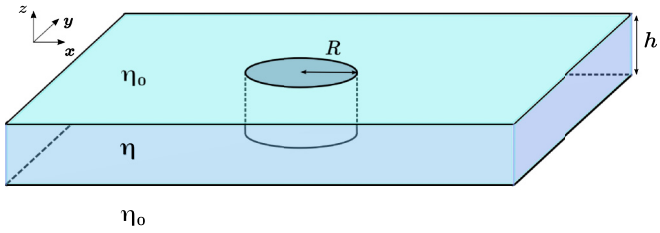

FIG. 1. (Color online) Sketch of the disk geometry.

The disks propel themselves in the plane of the film by means of an active "squirming" motion, achieved by a

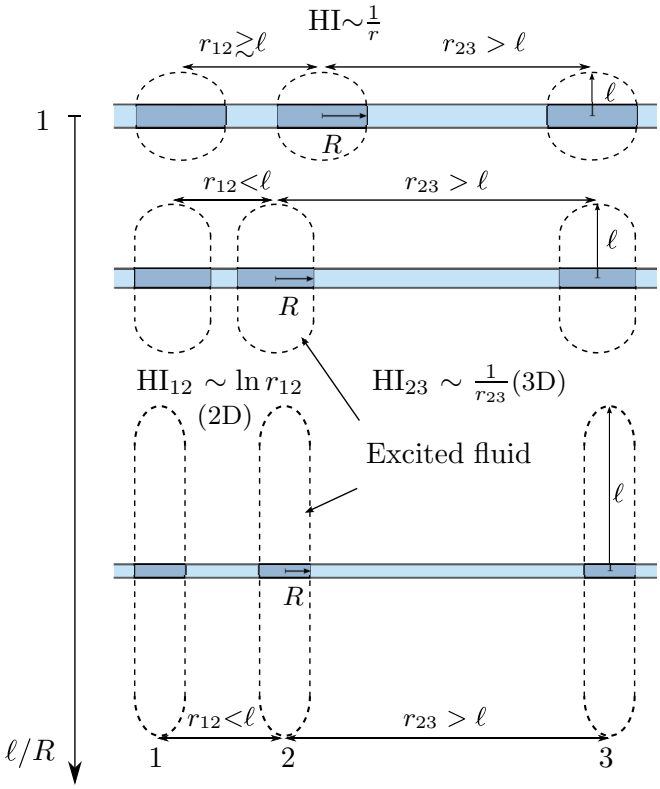

FIG. 2. (Color online) Schematic of effective description of the hydrodynamic interactions (HI in the figure), i.e., fluid velocities in the film generated by a point force on the disk boundaries. The fluid in the bulk is excited by motion in the film, and the Saffman length ℓ sets the extent of the bulk fluid set in motion. The region of bulk fluid excited by a disk of radius R can be viewed as a "ghost" particle, and the size of the ghost particles controls the crossover between 2D and 3D nature of the effective interactions [30–33]. When $\ell \leqslant R$, the effective hydrodynamic interactions (HI) between the disks separated by distance r are 3D-like and always scale to leading order as $1/r$. When $\ell > R$, the effective hydrodynamic interactions between disks depend on the ratio of the distance between the disks and the Saffman length ℓ. For a pair of disks with centers at positions $\boldsymbol{r}_i, \boldsymbol{r}_j$, the hydrodynamic interaction (HI) between them is 3D-like if $r_{ij} = |\boldsymbol{r}_i - \boldsymbol{r}_j| \gg \ell$ and scales like $1/r_{ij}$ while it is 2D-like when $r_{ij} = |\boldsymbol{r}_i - \boldsymbol{r}_j| \ll \ell$ and scales like $\ln r_{ij}$.

prescribed tangential velocity

$$S(\theta-\alpha_p)=B_1\sin(\theta-\alpha_p)+\tfrac{1}{2}B_2\sin 2(\theta-\alpha_p) \quad (1)$$

around the disk edges. We denote by β the ratio B_2/B_1 of the first to second modes in this expression. Positive β gives "pullers," and negative β gives "pushers."

With these dynamics, a single disk undisturbed by any others has, in an infinite box, a swim speed $v_0=B_1/2$ [25], with an instantaneous swim direction $\hat{\boldsymbol{e}}_p=(\cos\alpha_p,\sin\alpha_p)$, for the pth disk. In a suspension of many disks the actual swim speeds and directions evolve over time due to hydrodynamic interactions mediated by the Newtonian fluids surrounding the particles.

In the fluid above and below the film the velocity and pressure fields $\boldsymbol{v}'(\mathbf{r},t)$ and $p'(\mathbf{r},t)$ obey the mass balance condition for incompressible flow

$$0=\nabla\cdot\boldsymbol{v}'(\mathbf{r},t) \quad (2)$$

and the Stokes condition of force balance in the limit of creeping flow:

$$0=\eta_0\nabla^2\boldsymbol{v}'(\mathbf{r},t)-\nabla p'(\mathbf{r},t). \quad (3)$$

Here $\mathbf{r}=(x,y,z)$ denotes space and t time.

The fluid in the film has velocity and pressure fields $\boldsymbol{v}(\boldsymbol{r},t)$ and $p(\boldsymbol{r},t)$ that are taken to obey the mass balance condition for incompressible flow

$$0=\nabla_\perp\cdot\boldsymbol{v}(\boldsymbol{r},t) \quad (4)$$

and the force balance condition

$$0=\eta\nabla_\perp^2\boldsymbol{v}(\boldsymbol{r},t)-\nabla_\perp p(\boldsymbol{r},t)+\boldsymbol{f}+\boldsymbol{\sigma}^+-\boldsymbol{\sigma}^-, \quad (5)$$

where $\boldsymbol{r}=(x,y)$ are position vectors in the plane of the film. Here we have decomposed the gradient operator as $\nabla=(\nabla_\perp,\partial_z)$, with $\nabla_\perp$ representing gradients in the plane of the film.

We recognize Eq. (5) as a 2D Stokes equation subject to additional source terms $\boldsymbol{f}$, $\boldsymbol{\sigma}^\pm$. We choose the term $\boldsymbol{f}$ to represent forces around the edge of each disk:

$$\boldsymbol{f}(\boldsymbol{r},t)=\sum_p \boldsymbol{f}_p(\theta_p)\delta(r_p-R). \quad (6)$$

In this expression we are summing over the separate polar coordinate systems (r_p,θ_p) of the disks, such that for the pth term

$$\boldsymbol{r}=\boldsymbol{R}_p(t)+r_p\cos(\theta_p)\hat{\boldsymbol{x}}+r_p\sin(\theta_p)\hat{\boldsymbol{y}}, \quad (7)$$

in which $\boldsymbol{R}_p=\boldsymbol{R}_p(t)$ is the position of the center of the pth disk. These forces are included so as to ensure that the pth disk has at any instant a velocity around its edge

$$\boldsymbol{v}_p=\boldsymbol{V}_p-R\Omega_p\hat{\boldsymbol{\theta}}_p+S(\theta-\alpha_p)\hat{\boldsymbol{\theta}}_p, \quad (8)$$

comprising solid body translation and rotation, plus the tangential squirming motion prescribed by the slip velocity function in Eq. (1).

The integral properties of the forces are constrained to ensure zero total force and torque for each disk, consistent with these particles being swimmers driven by their own internal dynamics, and not subject to externally imposed force monopoles.

For mathematical convenience the interior of the discs is also taken to contain Newtonian fluid obeying Eqs. (4) and (5). We then simply discard this part of the solution as we are interested only in the part of the solution outside the discs.

We note that more general squirmer models could be studied with squirming velocity profiles prescribed for the interior points at the top and bottom surfaces as well as the edges, with the inclusion of a corresponding distribution of point forces on the two surfaces to ensure the prescribed boundary condition. This would be required, for example, if one wanted a solid interior of the disk, which our model does not address. However, we note that even for disks with a solid interior, the model studied here is a good approximation in the limit of $R\ll\ell$ though it is clearly not valid in this case for arbitrary values of $\epsilon=R/\ell$.

Finally, coupling between the film and the surrounding bulk fluid is achieved by setting

$$\boldsymbol{\sigma}^\pm=\eta_0\partial_z\boldsymbol{v}'|_{x=\pm h/2} \quad (9)$$

at the top and bottom of the disks. In this way, the source terms $\boldsymbol{\sigma}^\pm$ in Eq. (5) represent drag on the disks by the fluid flow in the bulk just above and below the film.

In the context of active particles, the Péclet number Pe is defined as the time taken for a particle thermally to diffuse a distance equal to its own radius, divided by the time taken for it to swim the same distance. Here we assume this to be infinite, as in Refs. [20–22], suppressing Brownian motion entirely and considering only the deterministic hydrodynamics defined above. Physically, this is the relevant limit for many active suspensions of, e.g., swimming bacteria. In simulations of active Brownian particles the tendency for phase separation is actually most pronounced in this limit [22]. The fact that we show hydrodynamics to suppress phase separation in this limit where, without hydrodynamics, it would be most pronounced gives strong evidence that hydrodynamics should further suppress phase separation across the full range of Péclet number.

As documented in Ref. [34], the case of strictly athermal, strictly hard sphere colloids with hydrodynamics is a singular limit. To avoid this unphysical pathology we consider the physically realistic case of slightly soft particles with a pairwise repulsive force $\boldsymbol{F}_{ij}=-f(a^3-a^2)\hat{\boldsymbol{d}}_{ij}$, $a=2sR/(d_{ij}-2R)$ for interparticle separation $d_{ij}<2R(1+s)$ between particles i and j. The effective area fraction is then $\phi=P\pi R^2(1+s)^2/L_xL_y$.

C. Active Brownian particles

Following Refs. [21,22,35–37] we take our active Brownian disks to obey translational dynamics

$$\dot{\boldsymbol{r}}_i=v_0\hat{\boldsymbol{e}}_i+\mu\boldsymbol{F}_{ij}, \quad (10)$$

again with swim speed v_0 for a single undisturbed particle. Their angular dynamics is prescribed by

$$\dot{\theta}_i=n_i(t),\langle n_i(t)n_j(t')\rangle=2\nu_r\delta_{ij}\delta(t-t'). \quad (11)$$

In contrast to the squirmers, the swim directions of the active Brownian particles are unaffected by interparticle interactions: they independently follow Eq. (11), regardless of the frequency or closeness of interparticle encounters.

Use of the word Brownian should be interpreted carefully in this context. In the dynamics just prescribed, only the angular motion is stochastic: the translational motion comprises deterministic swimming with slightly soft repulsive interactions between the particles. In any truly thermal system, the angular and translational diffusion coefficients would be related by a fluctuation dissipation relation. In contrast, the stochastic angular dynamics used here is not intended to represent true thermal motion, but a continuous time model of, e.g., stochastic run-and-tumble events. We use the word Brownian for consistency with the description of this angularly stochastic dynamics in the existing literature.

III. SIMULATION METHOD

In this section we outline our simulation method for the hydrodynamic squirmers. (Brownian particles are in comparison far easier to simulate, using standard methods that we do not discuss here.) For simplicity we introduce the method first in the context of the 2D case $\epsilon = \eta_0 R/\eta h \to 0$ of infinitely long cylinders propelling themselves in the plane of their cross section through a Newtonian solvent of viscosity η by means of the slip function $S(\theta)$, which is independent of height z along the cylinder. (For spherical particles, methods related to ours can be found in Refs. [26,28,34,38–41].) Extension to the 3D case of small but nonzero ϵ, representing disks in a highly viscous film, can then be shown to follow by relatively a simple modification.

The basis of the simulation method is to calculate at any time step, given the known current positions $\boldsymbol{R}_p$ and preferred swim directions α_p of all the particles, the forces required in Eq. (6) to effect the correct edge slip velocity functions S for each particle in Eq. (8), subject to the constraints of zero force and torque on each swimmer. Emerging from this calculation at each time step are then the center of mass translational and angular velocities for each particle $\boldsymbol{V}_p, \Omega_p$ in Eq. (8), which are used to update the particle positions and swim directions.

To implement this, we define the velocity vector

$$\boldsymbol{U}_{pq} = (v_{prqs}, v_{prqc}, v_{p\theta qs}, v_{p\theta qc})^T \tag{12}$$

in which v_{prqs} is the Fourier component in $\sin(q\theta_p)$ of the radial component of velocity around the edge of the pth disk and v_{prqc} the corresponding cosine mode. The quantities $v_{p\theta qs}, v_{p\theta qc}$ are their counterparts for the angular velocity components. In the same way we define the vector of force components

$$\boldsymbol{F}_{pq} = (f_{prqs}, f_{prqc}, f_{p\theta qs}, f_{p\theta qc})^T. \tag{13}$$

To obtain a relation between (12) and (13) we start by taking the curl and plane Fourier transform $(x,y) \to (k_x,k_y)$ of Eq. (5):

$$\eta k^4 \psi(\boldsymbol{k}) = [\boldsymbol{k} \wedge \boldsymbol{f}(\boldsymbol{k})] \cdot \hat{\boldsymbol{z}}. \tag{14}$$

(For infinite cylinders, the end-drag terms $\boldsymbol{\sigma}^{\pm}$ are absent.) Here ψ is the usual stream function, which guarantees that the incompressibility condition, Eq. (4), is satisfied.

It is then possible exactly to express $\boldsymbol{U}_{pq}$ in terms of the stream function $\psi(\boldsymbol{k})$, and likewise $\boldsymbol{F}_{pq}$ in terms of $\boldsymbol{k} \wedge \boldsymbol{f}(\boldsymbol{k})$. Together with Eq. (14), this gives

$$\boldsymbol{U}_{pq} = \sum_{p'=1}^{P} \sum_{q'=0}^{Q} \boldsymbol{M}_{qq'}(\boldsymbol{R}_p - \boldsymbol{R}_{p'}) \cdot \boldsymbol{F}_{p'q'} \tag{15}$$

in which $\boldsymbol{M}_{qq'}(\boldsymbol{R}_p - \boldsymbol{R}_{p'})$ is a matrix propagator that exactly relates the q'th Fourier mode of ring forces for a disk centered at $\boldsymbol{R}_{p'}$ to the qth mode of disk edge velocities of a disk centered at $\boldsymbol{R}_p$. It contains a sum over N_k plane Fourier modes for each of k_x and k_y. For numerical convenience it is calculated once over a grid of N_r, N_θ points, then at each time step of each run looked up by interpolation as needed.

At each numerical time step we solve Eq. (15) given the set of current disk locations $\boldsymbol{R}_p(t)$ and preferred swimming angles $\alpha_p(t)$, which feature in $\boldsymbol{U}_{pq}$. Prior to solution, the modes of the imposed squirming function for each disk are known in $\boldsymbol{U}_{pq}$, while the translational and rotational velocity of each disk are unknown. Conversely the forces modes are unknown, apart from the constraints of zero net force and torque for each disk. After transferring all knowns to the right-hand side and unknowns to the left-hand side, we then invert Eq. (15) to find the unknowns. The particle positions and swim angles are then updated as $\boldsymbol{R}_p \to \boldsymbol{R}_p + Dt\boldsymbol{V}_p, \alpha_p \to \alpha_p + Dt\Omega_p$, with time step Dt.

In the limit $Q \to \infty$, $N_k \to \infty$, $N_r \to \infty$, $N_\theta \to \infty$ this gives an *exact* solution of the *full* hydrodynamics of the 2D case of squirming cylinders in a periodic box of dimensions L_x, L_y. Emergent effects include the net propulsion of each disk, power law far-field interactions, and lubrication forces in near field. In numerical practice, Q, N_k, N_r, N_θ are of course finite, representing the maximum number of modes used in the simulation. Repeating the simulation for progressively larger Q, N_k, N_r, N_θ ensures convergence on these parameters to the desired limit $Q \to \infty$, $N_k \to \infty$, $N_r \to \infty$, $N_\theta \to \infty$.

In the 2D limit just discussed, a single such cylinder subject to a net external force in the plane of its cross section would suffer Stokes's paradox. In practice, of course, any such catastrophe is avoided here by the fact that each squirmer is free of any net force monopole, experiencing only higher multipoles of force generated by its own internal squirming dynamics.

Nonetheless, purely 2D hydrodynamics is still to be treated with caution. Accordingly, we also consider the 3D case of small but nonzero $\epsilon = R/\ell$, which corresponds to disklike particles moving in a highly viscous film, surrounded by a bulk fluid of much lower viscosity on either side. In this case the hydrodynamic interactions between the disks can be shown to follow, in the "Saffman" limit [30] of small ϵ, by means of a simple modification to the propagator in Eq. (15). The main effect of this is to modulate the far-field power law index by one (which would in fact remove Stokes paradox even if our particles were subject to external forces). Accordingly, once the 2D (cylinder) code has been written, the 3D (disks in a film) case follows by a straightforward modification of the propagator.

IV. PARAMETER VALUES AND UNITS

The squirmer model has nine parameters: the number of disks P; the disk radius R; the box size $L_x = Ł_y = L$ in the x-y

plane; the single particle swim speed v_0; the amplitude f of the repulsive potential; the range s of the repulsive potential; the Newtonian viscosity η; the ratio $\beta = B_2/B_1$; and the Saffmann parameter $\epsilon = \eta_0 R/\eta h$.

The active Brownian model has eight parameters, including P, R, L, v_0, f, and s, as for the squirmers. We then further have the drag coefficient μ (analogous to the Newtonian viscosity for the squirmers), and the ratio $\zeta = v_0\sqrt{P}/v_r L$ of the prescribed time of decorrelation of swim direction and the characteristic time interval between particle collisions.

In each case the number of independent parameters is reduced by three by choosing units of length in which the box size $L = 1$, of time in which the single particle swim speed $v_0 = 1$, and mass in which $\eta = 1$ (squirmers) or $\mu = 1$ (Brownian).

For both squirming and Brownian dynamics we then take the number of particles $P = 128$ or $P = 256$, heavily constrained by computational cost for the squirmers, with these P values being comparable to that achieved in other squirmer studies [26]. Much larger values of P are achievable for the Brownian disks, but we present results only for the same values of P as for the squirmers to ensure as direct a comparison as possible. We have checked that all the phenomena reported here are robust to changing between $P = 128$ and $P = 256$.

For both squirming and Brownian dynamics the repulsive potential has $f = 1, s = 0.1$ to ensure the dimensionless parameter $v_0/\mu f$ (and its counterpart in the squirming case) prescribing the small extent to which particles explore the interparticle repulsive potential is comparable to that in Ref. [21], giving almost hard disks. We have checked that our results are robust to reasonable variations in the value of s.

We have found the ratio $\beta \equiv B_2/B_1 = 0$ for the squirmers to be unimportant for the phase separation phenomenon of interest in this work. Accordingly, we show results below only for the case $\beta = 0$. However, we have verified that our result showing suppression of phase separation holds across a wide range of values of $\beta = -\infty, -5, -1, 0, +1, +5, +\infty$ (with $-\infty$ and $+\infty$ actually equivalent for this model).

This leaves just two dimensionless parameters to be explored numerically in each case. For the squirmers we have the area fraction $\phi = P\pi R^2(1+s)^2/L^2$, and the Saffmann parameter $\epsilon = \eta_0 R/\eta h$. For the Brownian disks we have the area fraction ϕ, as for the squirmers, and the ratio $\zeta = v_0\sqrt{P}/v_r L$ of the prescribed time of decorrelation of swim direction and the characteristic time between particle collisions.

V. MEASURED QUANTITIES

Here we define the various statistical quantities that we shall report in the results section below:

(1) The swim speed

$$v = \frac{1}{PT}\int_0^T \sum_{p=1}^{P} |v_p(t)|, \tag{16}$$

averaged over the ensemble of particles $p = 1, \ldots, P$ and over a time interval $t = 0 \to T$ large enough to get good statistics. Note that this measure of speed we choose to adopt differs slightly from the choice in Ref. [21], extracted from the early-time ballistic regime of the mean squared particle displacement, which one can show analytically is equivalent to $[\frac{1}{PT}\int_0^T \sum_i |v_i(t)|^2]^{1/2}$.

(2) The scaled number fluctuations $\delta_N = \Delta N/N^{1/2}$ in a region of the sample with average number of particles N. To measure this we divide the sample into $b = 1, \ldots, B = P/N$ equally sized boxes, define the time averages $\bar{n_b}, \bar{n_b^2}$ of the number and squared number of particles in the bth box, then report

$$\delta_N = \frac{1}{B\sqrt{N}} \sum_{b=1}^{B} \sqrt{\bar{n_b^2} - \bar{n_b}^2}. \tag{17}$$

(3) The characteristic time τ_o for the decorrelation of particle swim direction, defined as the time interval $\Delta t = \tau_o$ for the correlation function

$$P(\Delta t) = \frac{1}{PT}\int_0^T dt \sum_p \boldsymbol{e}_p(t+\Delta t)\cdot\boldsymbol{e}_p(t) \tag{18}$$

to fall to $1/e$.

(4) The time between interparticle collisions, for which we find a reasonable definition to be

$$\tau_c = \pi R/(v_0 - \tilde{v}), \tag{19}$$

in which

$$\tilde{v} = \frac{1}{PT}\int_0^T \sum_p \boldsymbol{v}_p(t)\cdot\boldsymbol{e}_p(t) \tag{20}$$

is a measure of the extent to which a particle manages actually to attain its full velocity in its attempted swim direction. The degree to which this differs from the free swim speed is a measure of the degree to which scattering occurs. We checked by direct observation that τ_c provides a reliable measure at low area fraction. At high area fraction this comparison is more difficult to carry out, because particles slither around each other continuously.

VI. RESULTS

We explore first active Brownian disks in the regime where the particle swim direction is slow to decorrelate, $\zeta \gg 1$. We do this to establish a point of contact with earlier simulation studies [21] of active Brownian disks, which were performed in this regime, to provide a context in which to discuss our results below.

As seen in Fig. 3 (top), and correspondingly in Fig. 3 of Ref. [21] (though there with a much larger $P = 10^4$), the particle swim speed v decreases strongly with area fraction ϕ. Accordingly this system is a good candidate for MIPS via the (a)–(b) feedback mechanism discussed above. The expected spinodal, according to the instability criterion $d\log v/d\log\phi < -1$ of Refs. [18,19], is located at the vertical dotted line in Fig. 3.

Phase separation is indeed observed: see the top two snapshots of Fig. 4, and correspondingly Fig. 1 of Ref. [21]. This is reflected also in enhanced number fluctuations: our plot of $\delta_N(N)$ for each ϕ (not shown) shows all the same features as Fig. 3 of Ref. [37], though obviously cuts off sooner at high N

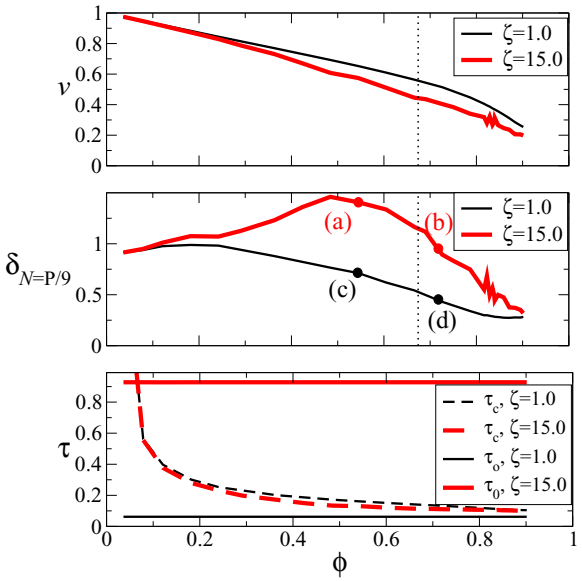

FIG. 3. (Color online) Active Brownian particles. Top: Average particle speed as a function of average particle area fraction. Expected spinodal shown by dotted line. Middle: Scaled number fluctuations. Bottom: Characteristic time τ_o for reorientation of particle swim direction and interparticle collision time τ_c.

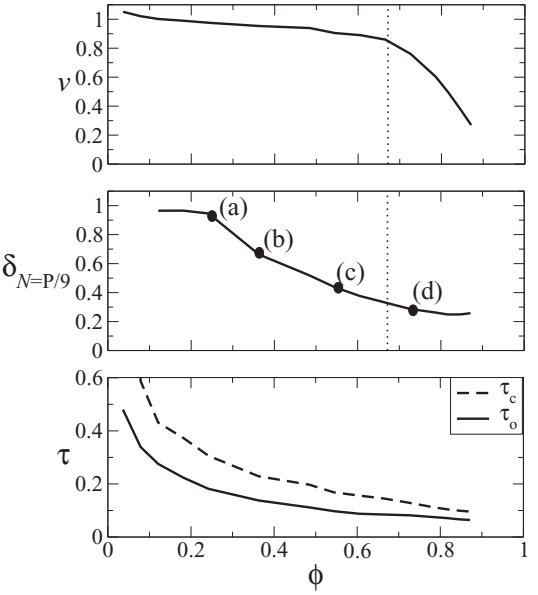

FIG. 5. Hydrodynamic squirmers (cylinders). Top: Average particle speed as a function of average particle area fraction. Expected spinodal shown by dotted line. Middle: Scaled number fluctuations. Bottom: Characteristic time τ_o for reorientation of particle swim direction and interparticle collision time τ_c.

due to our smaller number of simulated particles P. Reporting in Fig. 3 (middle) the single value $\delta_{N=P/9}$, close to the peak of $\delta_N(N)$ for this value of P, clearly indicates separation with binodal onset around $\phi = 0.25$.

Consider now the hydrodynamic squirmers. We start for simplicity with the 2D case $\epsilon = 0$ (cylinders), our results for which are shown in Fig. 5. As for the Brownian disks the ensemble average swim speed declines strongly with particle area fraction, suggesting that MIPS should again occur via the (a)–(b) feedback outlined above, with spinodal onset at the vertical dotted line according to the criterion $d \log v / d \log \phi < -1$ of Ref. [18]. Remarkably, however, we find no evidence for bulk phase separation in the 2D squirmers: see the snapshots of Fig. 6 and the correspondingly suppressed number fluctuations $\delta_{N=P/9}$ in Fig. 5 (middle panel). We do,

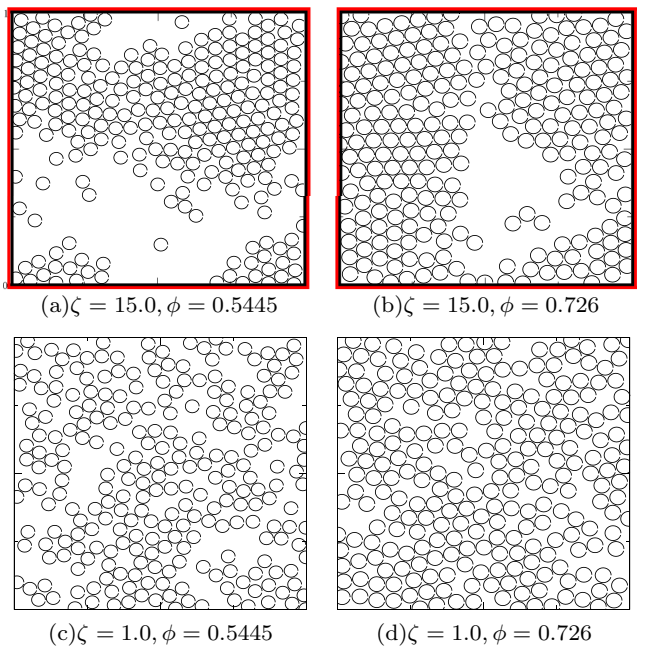

FIG. 4. (Color online) Snapshots for active Brownian particles, corresponding to circles (a)–(d) in Fig. 3.

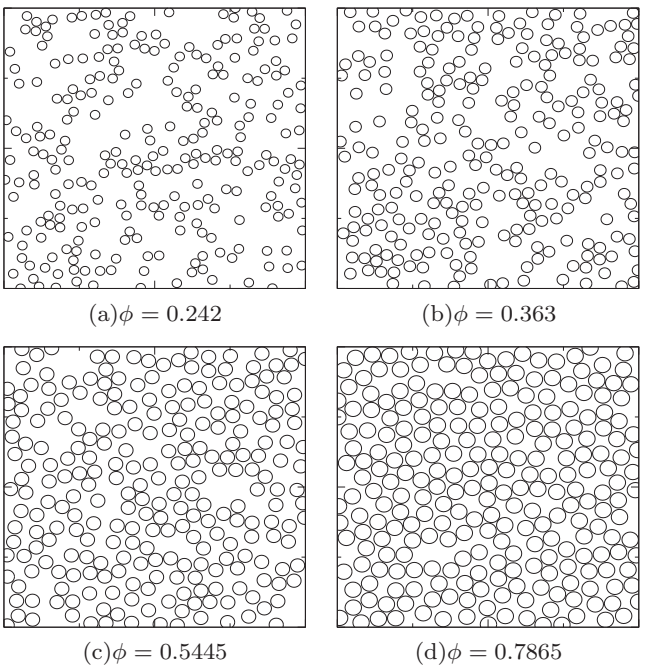

FIG. 6. Snapshots for hydrodynamic squirmers, corresponding to circles (a)–(d) in Fig. 5.

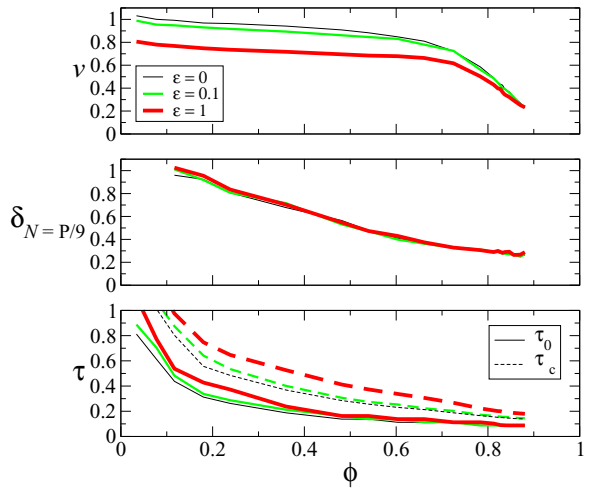

FIG. 7. (Color online) Hydrodynamic squirmers (disks). Top: Average particle speed as a function of average particle area fraction. Middle: Scaled number fluctuations. Bottom: Characteristic time τ_o for reorientation of particle swim direction and interparticle collision time τ_c.

however, find a tendency to form small stringlike clusters at low area fractions, as reported previously by other authors [26].

To check that this result is not particular to the case of 2D hydrodynamics discussed so far, $\epsilon = 0$, we show counterpart results for the case of small but nonzero ϵ in Fig. 7. As discussed above, this corresponds to the 3D hydrodynamics of disks squirming in a film of highly viscous fluid, surrounded above and below by a bulk fluid of much lower viscosity. As can be seen, there is no evidence of phase separation in this case either. Corresponding state snapshots (not shown) closely resemble those in Fig. 6 for the cylinders, again showing no evidence of phase separation.

All these squirmer simulations were run for long times (typically $t_{max} = 20.0$, which in our units is the time taken for any free squirmer to cross the entire simulation box 20 times). In each case, we checked the run was long enough to ensure that all the statistical quantities defined above had convincingly reached a steady state.

VII. DISCUSSION

To understand how hydrodynamics might cause this suppression of motility-induced phase separation (MIPS) we now revisit the original argument for MIPS, as first put forward in the context of run-and-tumble dynamics and later generalized to other systems.

Model run-and-tumble particles move in a series of straight line runs at a constant speed v_0, when dilute, between tumbles in which they rapidly reassign their swim direction. These tumbles occur randomly with a typical intertumble time interval α^{-1}. The argument for phase separation stemming from this motility is as follows: (a) It can be shown that the local particle area fraction in any small region of fluid scales inversely with the local swim speed v. (Although intuitively reasonable, this is in fact a strongly nonequilibrium effect stemming from activity.) (b) It is assumed that between tumbles particles move more slowly in regions of high volume fraction, being impeded by crowding, rendering the swim speed a decreasing function of volume fraction $v(\phi) < v_0$. Positive feedback between (a) and (b) gives phase separation, onset with spinodal instability from an initially homogeneous state when $d \log v / d \log \phi < -1$. This argument extends to active Brownian particles of angular diffusivity ν_r, with an exact mapping $\alpha \to (d-1)\nu_r$ in d dimensions [20].

Consider carefully part (b) of this argument. In order meaningfully to define an intertumble swim speed $v(\phi) < v_0$ that is reduced by crowding, each particle must encounter many other particles between tumbles: the characteristic intertumble time α^{-1} must be large compared to the characteristic time scale τ_c between collisions. Transcribing this reasoning to Brownian particles, the angular diffusion time must be small compared to τ_c. Generalizing still further, we propose that regardless of the underlying microscopic dynamics (run and tumble, Brownian, or hydrodynamic) the decay time τ_o of the swim-direction autocorrelation function must greatly exceed the interparticle collision time scale τ_c if part (b) of the argument is to hold and MIPS is to occur.

With this reasoning in mind consider again Fig. 3 for Brownian disks in the regime $\zeta \gg 1$ discussed above. The bottom panel of this figure shows the decay time τ_o of the autocorrelation function of particle swim direction, together with the typical time τ_c between particle collisions. Consistent with the externally imposed angular diffusivity ν_r being small in these runs (large $\zeta = 15$), τ_o is a relatively large constant across all ϕ. Except in the very dilute limit each particle encounters many others during the time it takes to alter its swim direction: $\tau_c \ll \tau_o$. Between angular reorientation events, then, each particle properly samples the ensemble average reduced swim speed $v(\phi) < v_0$: part (b) of the feedback loop holds and MIPS can indeed occur, as observed. Indeed, this mean-field nature of $v(\phi)$ was noted in Ref. [20].

In contrast, for the squirmers we are not at liberty to prescribe from the outset the timescale τ_o of decorrelation of particle swim direction: instead this emerges naturally as a result of hydrodynamic interactions between the particles, which are *a priori* unknown. (Put differently, there is no externally tunable ζ for these particles.) Indeed, two-squirmer studies show that with hydrodynamics each scattering event ("collision") typically results in an $O(1)$ change in swim direction for each particle involved. Accordingly, in these many-squirmer simulations we expect $\tau_o \approx \tau_c$. This is indeed observed: see Fig. 5 (bottom panel). Squirmers will therefore be unable properly to sample the reduced $v(\phi) < v_0$ between reorientation events: part (b) of the feedback argument fails, and MIPS is suppressed.

To support this argument we finally revisit the Brownian disks, but now imposing a smaller $\zeta = 1.0$ so that the particles reorient their swim directions much more quickly than in the large ζ case discussed above, giving dynamics more closely akin to the squirmers ($\tau_o \approx \tau_c$, Fig. 3, bottom). Phase separation is then indeed strongly suppressed: see the bottom two snapshots of Fig. 4 and the significantly reduced number fluctuations of Fig. 3 (middle panel). This is despite the ensemble average velocity $v(\phi)$ still decreasing strongly enough for this $\zeta = 1.0$ to satisfy the condition for spinodal onset. Put simply, particles that rapidly reorient do not have time to sample this mean field $v(\phi)$ between reorientation events.

Our findings are consistent with an earlier comment in Ref. [42] that a tendency to order was suppressed by hydrodynamics in a suspension of rodlike swimmers; with experiments demonstrating highly cooperative dynamics and mesoscale turbulence in living fluids, without associated evidence for phase separation [43]; and with experiments [44] demonstrating that concentrated bacterial suspensions are dominated by a competition between short range lubrication and steric effects.

Despite the absence of true bulk phase separation for the squirmers, and for the Brownian disks with $\tau_o \approx \tau_c$, some particle clustering is nonetheless still apparent in Figs. 4(c) and 4(d) and Figs. 6(a)–6(d). Whether this clustering can be interpreted in terms of a nearby but suppressed MIPS, which could therefore be a generic feature of active matter with hydrodynamics, remains an open question.

VIII. CONCLUSIONS

We have simulated with hydrodynamics a suspension of active squirming disks across the full range of area fractions from dilute to close packed. In doing so we have shown that hydrodynamic interactions strongly suppress motility induced phase separation. These findings should apply generically to active systems in which hydrodynamics are important, and in which the effective particle velocity depends on volume fraction via collisions impeding particle motion. Obvious exceptions include systems in which v depends on ϕ instead by chemically mediated mechanisms (such as quorum sensing [45]), allowing MIPS to arise at relatively low volume fractions, and/or systems in which the particles reside in (or on the surface of) a gel [46].

Open for further study is the degree to which particle elongation might force a correlation of particle orientations, potentially restoring phase separation for sufficiently elongated particles, and so possibly even bringing an understanding of phase separation in active rodlike suspensions [7,9,17] into the framework proposed here. Also unresolved remains the effect of dimensionality of particle packing and hydrodynamic propagator: 3D packings with 3D hydrodynamics do not appear to phase separate [26], nor do the 2D packings with 2D hydrodynamics (cylinders) or 3D hydrodynamics (disks) reported here. However, studies of 2D packings of spherical particles with 3D hydrodynamics [28] did report separation, though at an area fraction $\phi = 0.1$ that seems very low for MIPS to be implicated. This issue of dimensionality deserves careful future attention. It also remains an open challenge to address the clustering observed experimentally in synthetic colloids [11], noting that (true) interparticle attractions cannot be entirely eliminated experimentally. Such questions notwithstanding, the mechanism proposed here is expected to arise widely in active matter, and particularly in active colloids, which form the focus of intense current experimental interest [10,11].

Note added in proof. We note that recently a related work was published by Zöttl and Stark [47] studying a squirmer suspension confined between plates separated by a distance comparable to the swimmer size. What differentiates our work from theirs is the fact that hydrodynamic interactions under confinement are effectively screened with a screening length that is set by the gap size. In our study of an extended and *unconfined* system, hydrodynamic interactions are always long ranged, while the thin film geometry allows us to tune the effective dimensionality of the long-ranged hydrodynamic interactions to make a smooth crossover from 2D to 3D behavior.

ACKNOWLEDGMENTS

We thank Mike Cates, Paul Chaikin, and Oliver Harlen for discussions. The research leading to these results has received funding from the European Research Council under the European Union's Seventh Framework Programme (FP7/2007-2013)/ERC Grant agreement No. 279365. We thank the KITP for hospitality while some of this work was done: this research was supported in part by the National Science Foundation under Grant No. NSF PHY11-25915.

[1] M. C. Marchetti *et al.*, Rev. Mod. Phys. **85**, 1143 (2013), and references therein.
[2] F. Jülicher, K. Kruse, J. Prost, and J.-F. Joanny, Phys. Rep. **449**, 3 (2007).
[3] M. Poujade *et al.*, Proc. Nat. Acad. Sci. USA **104**, 15988 (2007).
[4] H. C. Berg, *E. coli in Motion* (Springer, New York, 2003).
[5] S. Rafai, L. Jibuti, and P. Peyla, Phys. Rev. Lett. **104**, 098102 (2010).
[6] J. K. Parrish and W. M. Hamner, *Three Dimensional Animal Groups* (Cambridge University Press, Cambridge, 1997).
[7] V. Narayan, S. Ramaswamy, and N. Menon, Science **317**, 105 (2007).
[8] A. Kudrolli, G. Lumay, D. Volfson, and L. S. Tsimring, Phys. Rev. Lett. **100**, 058001 (2008).
[9] J. Deseigne, O. Dauchot, and H. Chate, Phys. Rev. Lett. **105**, 098001 (2010).
[10] G. Ruckner and R. Kapral, Phys. Rev. Lett. **98**, 150603 (2007); J. R. Howse, R. A. L. Jones, A. J. Ryan, T. Gough, R. Vafabakhsh, and R. Golestanian, *ibid.* **99**, 048102 (2007); J. Palacci, C. Cottin-Bizonne, C. Ybert, and L. Bocquet, *ibid.* **105**, 088304 (2010); A. Erbe, M. Zientara, L. Baraban, C. Kreidler, and P. Leiderer, J. Phys.: Condens. Matter **20**, 404215 (2008); W. Paxton *et al.*, J. Am. Chem. Soc. **126**, 13424 (2004); Y. Hong, N. M. K. Blackman, N. D. Kopp, A. Sen, and D. Velegol, Phys. Rev. Lett. **99**, 178103 (2007); H.-R. Jiang, N. Yoshinaga, and M. Sano, *ibid.* **105**, 268302 (2010); G. Volpe *et al.*, Soft Matter **7**, 8810 (2011); S. Thutupalli, R. Seemann, and S. Herminghaus, New J. Phys. **13**, 073021 (2011); R. Golestanian, T. B. Liverpool, and A. Ajdari, *ibid.* **9**, 126 (2007); Phys. Rev. Lett. **94**, 220801 (2005).

[11] I. Theurkauff, C. Cottin-Bizonne, J. Palacci, C. Ybert, and L. Bocquet, Phys. Rev. Lett. **108**, 268303 (2012); O. Chepizhko, E. G. Altmann, and F. Peruani, *ibid.* **110**, 238101 (2013); J. Palacci *et al.*, Science **339**, 936 (2013).
[12] J. Toner and Y. Tu, Phys. Rev. E **58**, 4828 (1998).
[13] J. Toner and Y. Tu, Phys. Rev. Lett. **75**, 4326 (1995).
[14] S. Ramaswamy, R. Simha, and J. Toner, Europhys. Lett. **62**, 196 (2003).
[15] J. Toner, Y. Tu, and S. Ramaswamy, Ann. Phys. **318**, 170 (2005).
[16] A. Baskaran and M. C. Marchetti, Phys. Rev. E **77**, 011920 (2008); Phys. Rev. Lett. **101**, 268101 (2008).
[17] H. Chate, F. Ginelli, and R. Montagne, Phys. Rev. Lett. **96**, 180602 (2006); H. Chate *et al.*, Eur. Phys. J. B **64**, 451 (2008).
[18] J. Tailleur and M. E. Cates, Phys. Rev. Lett. **100**, 218103 (2008).
[19] M. E. Cates, Rep. Prog. Phys. **75**, 042601 (2012).
[20] M. E. Cates and J. Tailleur, Europhys. Lett. **101**, 20010 (2013).
[21] Y. Fily and M. C. Marchetti, Phys. Rev. Lett. **108**, 235702 (2012).
[22] G. S. Redner, M. F. Hagan, and A. Baskaran, Phys. Rev. Lett. **110**, 055701 (2013).
[23] M. J. Lighthill, Comm. Pure Appl. Math. **5**, 109 (1952).
[24] J. R. Blake, J. Fluid Mech. **46**, 199 (1971).
[25] J. R. Blake, Bull. Austr. Math. Soc. **5**, 255 (1971).
[26] T. Ishikawa, J. Locsei, and T. Pedley, J. Fluid Mech. **615**, 401 (2008).
[27] F. Alarcón and I. Pagonabarraga, J. Mol. Liquids **185**, 56 (2013).
[28] T. Ishikawa and T. J. Pedley, Phys. Rev. Lett. **100**, 088103 (2008).
[29] D. Saintillan and M. J. Shelley, Phys. Rev. Lett. **99**, 058102 (2007); **100**, 178103 (2008); J. R. Soc. Interf. **9**, 571 (2012).
[30] P. G. Saffman, J. Fluid Mech. **73**, 593 (1976); P. G. Saffman and M. Delbruck, Proc. Natl. Acad. Sci. USA **72**, 3111 (1975).
[31] D. K. Lubensky and R. E. Goldstein, Phys. Fluids **8**, 843 (1996).
[32] A. J. Levine, T. B. Liverpool, and F. C. MacKintosh, Phys. Rev. Lett. **93**, 038102 (2004); Phys. Rev. E **69**, 021503 (2004).
[33] M. Leoni and T. B. Liverpool, Phys. Rev. Lett. **105**, 238102 (2010); Europhys. Lett. **92**, 64004 (2010).
[34] J. Melrose and R. Ball, Europhys. Lett. **32**, 535 (1995).
[35] J. Bialke, T. Speck, and H. Löwen, Phys. Rev. Lett. **108**, 168301 (2012).
[36] S. R. McCandlish, A. Baskaran, and M. F. Hagen, Soft Matter **8**, 2527 (2012).
[37] S. Henkes, Y. Fily, and M. C. Marchetti, Phys. Rev. E **84**, 040301 (2011).
[38] A. A. Evans, T. Ishikawa, T. Yamaguchi, and E. Lauga, Phys. Fluids **23**, 111702 (2011).
[39] J. W. Swan, J. F. Brady, R. S. Moore, and ChE 174, Phys. Fluids **23**, 071901 (2011).
[40] W. Hwang, M. Hulsen, and H. Meijer, J. Non-Newtonian Fluid Mech. **121**, 15 (2004).
[41] J. Brady and G. Bossis, Annu. Rev. Fluid Mech. **20**, 111 (1988).
[42] J. P. Hernandez-Ortiz, P. T. Underhill, and M. D. Graham, J. Phys.: Condens. Matter **21**, 204107 (2009).
[43] H. H. Wensink *et al.*, Proc. Nat. Acad. Sci. USA **109**, 14308 (2012).
[44] K. Drescher *et al.*, Proc. Nat. Acad. Sci. USA **108**, 10940 (2011).
[45] M. B. Miller and B. L. Bassler, Ann. Rev. Microbiol. **55**, 165 (2001).
[46] M. Cates, D. Marenduzzo, I. Pagonabarraga, and J. Tailleur, Proc. Nat. Acad. Sci. USA **107**, 11715 (2010); F. D. C. Farrell, M. C. Marchetti, D. Marenduzzo, and J. Tailleur, Phys. Rev. Lett. **108**, 248101 (2012); C. L. Liu *et al.*, Science **334**, 238 (2011); X. Fu, L.-H. Tang, C. Liu, J.-D. Huang, T. Hwa, and P. Lenz, Phys. Rev. Lett. **108**, 198102 (2012).
[47] A. Zöttl and H. Stark, Phys. Rev. Lett. **112**, 118101 (2014).